INTERNATIONAL JOURNAL OF HYDROGEN ENERGY 42 (2017) 28786–28796

Available online at www.sciencedirect.com

ScienceDirect

journal homepage: www.elsevier.com/locate/he

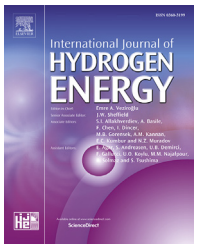

Carbon-supported Pt nanoparticles with (100) preferential orientation with enhanced electrocatalytic properties for carbon monoxide, methanol and ethanol oxidation in acidic medium

*R.M. Antoniassi, J.C.M. Silva, T. Lopes, A. Oliveira Neto, E.V. Spinacé**

Instituto de Pesquisas Energéticas e Nucleares – IPEN-CNEN/SP, Av. Prof. Lineu Prestes, 2242, Cidade Universitária, 05508-900 São Paulo, SP, Brazil

ARTICLE INFO

Article history:
Received 7 July 2017
Received in revised form
9 September 2017
Accepted 6 October 2017

Keywords:
Pt cubic nanoparticles
Pt(100)
CO-stripping
Ethanol and methanol electro-oxidation
PEMFC

ABSTRACT

The relationship between atomic arrangement (morphology) and catalytic activity/selectivity in heterogeneous catalysis is an actual hot research topic concerning a range of reactions. This article evaluates one-pot synthesized carbon-supported Pt nanoparticles with preferential Pt(100) orientation prepared with an environmentally friendly shape-directing agent and compares this with Pt/C polycrystalline towards CO, methanol and ethanol electrooxidation reactions. The preferentially cubic nanomaterial (Pt-(100)) interacts differently with CO molecule and presents distinct hydrogen adsorption/desorption characteristics. Pt/C polycrystalline exhibits a CO-stripping profile with one peak at 0.86 V in contrast to three peaks between 0.75 and 0.86 V and a pre-peak at about 0.4–0.6 V for the Pt/C-(100), which may be associated to the unique surface characteristics of the cubic material. The onset potentials towards carbon monoxide, methanol and ethanol electro-oxidation reactions on Pt/C-(100) are 22%, 21% and 54% lower than on Pt/C polycrystalline. The ratio between the forward per backward peak current densities for the electrooxidation of ethanol and methanol are higher on Pt/C-(100), which suggests that Pt(100) domains are more tolerant to undergo poisoning by the intermediates/by-products formed in these reactions. Proton exchange membrane fuel cells fed with pure hydrogen and with a H_2/CO mixture show superior performance using Pt/C-(100) as anode in comparison to Pt/C polycrystalline catalyst. These results evidence that controlling the morphology of Pt nanoparticles is a key factor to improve the catalytic activity of the polymer electrolyte fuel cell fueled with fuels that involve the electro-oxidation of CO.

* *Corresponding author*. Instituto de Pesquisas Energéticas e Nucleares - IPEN-CNEN/SP, Av. Prof. Lineu Prestes, 2242 – Cidade Universitária, 05508-900 São Paulo, SP, Brazil.
E-mail addresses: espinace@ipen.br, espinace@yahoo.com.br (E.V. Spinacé).
https://doi.org/10.1016/j.ijhydene.2017.10.036

Introduction

Proton exchange membrane fuel cells (PEMFC) have emerged as a promising alternative for an environmentally friendly power generation [1,2]. The PEMFC device can be fed with different fuels e.g. hydrogen, methanol and ethanol without the need of modifying its main structure [1–6]. Among the three cited fuels, hydrogen generates higher current densities. However, small amounts of CO present in the H_2 causes serious loss in the fuel cell efficiency, especially when platinum is used as anode [2,7,8]. It is important to point out that CO is a common contaminant when hydrogen is obtained by methane and methanol steam reforming, cheap sources of H_2 [2].

Methanol can be used as an alternative to hydrogen in PEMFCs and it presents some advantages which are related to storage and transportation, since it is a liquid fuel at room temperature [6,9]. Platinum is the element with the highest catalytic activity for methanol and hydrogen electro-oxidation. However, CO strongly adsorbs on the Pt nanoparticles surface [9,10], and reduces the efficiency of practical systems fed with methanol of H_2/CO by causing overpotential losses. The complete oxidation of methanol to CO_2 involves 6 electrons per methanol molecule, though CO is an intermediate for this complete oxidation [10,11], as a result, if the electrocatalyst utilized is sensitive to undergo poisoning by CO, severe losses are seen in the efficiency of direct alcohol fuel cells, for instance the methanol based device (direct methanol fuel cells – DMFCs) [9].

Ethanol has been recognized as a promising fuel for PEMFCs, given that it can be produced directly from the fermentation of biomass, which makes it a renewable fuel, leaving the natural balance of carbon dioxide in the atmosphere unaltered [12–14]. The thermodynamic potential value of 0.08 V (vs RHE) of the complete oxidation of ethanol to CO_2 enables its direct fueling in anodic fuel cells compartment [15]. As a result, Direct Ethanol Fuel Cell (DEFC) has attracted great attention. The use of ethanol directly as a fuel, when compared with hydrogen and methanol, shows some technical advantages, for instance, low-toxicity, relative high energy density, it can be easily stored in fuel tanks and can be produce from biomass [3,16,17]. However, a complete ethanol oxidation reaction (EOR) to CO_2 involving 12 electrons requires the cleavage of the C–C bond, which is a great challenge [18–20]. Additionally, considering the splitting of the C–C bond, CO is an intermediate for complete oxidation of ethanol to CO_2 [21], as it is for the complete oxidation of methanol. However, and as already described here, catalysts based on Pt nanoparticles anchored on carbon support, which are considered state of art for EOR in DEFCs, lack in low selectivity to completely oxidize ethanol to CO_2, as a result, acetaldehyde and acetic acid are the main oxidation products by a 2 and a 4 electrons mechanism. These mechanisms drastically diminish the cell electrical performance and efficiency [16,21].

This literature revision evidences that CO causes significant losses in the overall efficiency of PEMFCs when this is fed with hydrogen containing CO, methanol and ethanol. Furthermore, ethanol presents an additional challenge that is the cleavage of the C–C bond, which affects the efficiency of direct ethanol fuel cells. In order to overcome these problems, binary and multimetallic platinum-based materials have been proposed, e.g. PtSn, PtRu, PtRuSn [2,22,23]. Modifications on nanoparticles supports are also found for Pt-based catalysts [24–26]. On the other hand, there are studies focused on the control of the morphology of the metal nanoparticles to achieve preferential crystallographic facets on the surface, which is a simpler approach and has been shown to increase, by itself, the catalytic activity [6,10,27,28].

Housmans et al. [11] investigated the electro-oxidation of methanol on single crystals and found that the catalytic activity increases in the following order Pt(111) < Pt(110) < Pt(100). This is in agreement with Grozovski et al. [10], which showed that Pt(100) single crystals presents the highest catalytic activity for methanol electrooxidation. Han et al. [6] synthesized platinum nanocubes (using polyvinylpyrrolidone as stabilizer) with Pt(100) facets and reported that platinum nanocubes show higher catalytic than polycrystalline platinum towards methanol electro-oxidation. According to the authors, platinum nanocubes are less poisoned by adsorbed intermediates during the electro-oxidation of methanol in comparison to polycrystalline platinum nanoparticles.

Studies on the electrochemical oxidation of ethanol employing single crystals indicate that the cleavage of the C–C bond of the ethanol molecule is sensitive to the platinum facet. In acid media, Pt(100) electrodes with (100) and (111) defects favor the C–C cleavage, whereas the reaction on Pt(111) electrodes proceeds through an incomplete electro-oxidation mechanism. This mechanism tends to form acetic acid as a major product [29–32]. In the context of nanoparticles, Pt(100) is also more effective in promoting the scission of C–C bonds in comparison to Pt(111) [16,27,33], where platinum nanocubes, with Pt(100) facets, has shown a higher catalytic activity towards the electrooxidation of ethanol than polycrystalline Pt nanoparticles [6,27,34]. These prior literature results point that nanoparticles with preferential orientation could be a key factor on improving the catalytic activity of the materials. However, achieving a complete control of the nanoparticles surface crystallographic orientation is not always a simple task. Most of the nanoparticles presenting controlled shape reported in the literature involve the addition of stabilizing/shape orientation agents, such as polyvinylpyrrolidone (PVP), sodium polyacrilate, oleylamine [35,36] in the nanoparticle synthesis solution. The drawback of using these additive agents is that they severely block the activity sites of metal catalyst and require intensive chemical washing steps to completely remove them from the nanoparticle surface, which challenges the practical applicability of these approaches. However, recently, some of the present authors have discovered a facile and free of stabilizing agents strategy to produce supported Pt(100) faceted nanocubes by using only halide ions as shape directing agent [37]. It is noteworthy noting that these halides are easily removed from the catalyst by simply washing it with DI water. Herein, we demonstrate that this versatile Pt/C nanoparticle with preferential Pt(100) orientation presents suitably higher catalytic activity than Pt/C polycrystalline towards CO, methanol and ethanol electrooxidation reactions. Additionally, fuel cell experiments using H_2 and H_2/CO showed that this shape-

controlled Pt nanoparticle with (100) preferential orientation is less affected by the presence of CO in the H_2 stream than Pt/C polycrystalline. These results evidence that structural proprieties can effectively promote the catalytic performance of platinum achieving higher mass activities.

Experimental

The following materials were used: hydrated hexachloroplatinic (IV) acid ($H_2PtCl_6 \cdot 6H_2O$, 99.6% purity) as metal precursor, potassium bromide (KBr, 99.7%), Vulcan Carbon (X72R – Cabot Corporation), DI water and ethylene glycol (EG). The synthesis of carbon-supported Pt/C with Pt (100) preferential orientation (denoted as Pt/C-(100)) was conducted according to our previous work [37], by a modified alcohol reduction process. In a typical synthesis, a determined amount of carbon support was added to a solution containing EG/water (3/1, v/v), which was heated at 150 °C under a vigorous magnetic stirring. After the temperature was reached, 30 wt% of the Pt precursor was added and the resulting mixture was maintained under reflux for 20 min. KBr was quickly added (Br^-: Pt molar ratio of 300:1) and the mixture was kept under reflux for a further 20 min. Subsequently, the remainder 70 wt% of the Pt precursor was rapidly added and the reaction was allowed to proceed for more 150 min. Finally, the mixture was filtered and the obtained solid was washed with water to remove the impurities and dried at 80° for 2 h. For comparison purposes, polycrystalline Pt/C electrocatalyst (20 wt% of Pt) was prepared in a single step, without the addition of KBr.

Size and morphology of Pt nanoparticles were characterized by Transmission Electron Microscopy (TEM, JEOL – model JEM 2100F), operating at 200 kV. For TEM analyses, an amount of the electrocatalyst was suspended in isopropyl alcohol and dropped in a TEM copper grid coated with colloidal film. Platinum nanoparticles (PtNPs) size was measured by end-to-end particle extension. X-Ray Diffraction (XRD) was performed employing a Rigaku diffractometer, model Miniflex II, using a Cu kα radiation source (λ = 0,15406 nm). The XRD patterns were recorded in the range of 2Θ between 20 and 90°, with a step size of 0.05° and a scan rate of 2 s per step. Thermogravimetric Analysis (TGA) was performed in 25 mL min^{-1} of synthetic air, on the furnace temperature range of 5–800 °C.

Cyclic voltammograms were recorded to verify the occurrence of basal Miller planes on Pt/C polycrystalline and Pt/C-(100). The electrochemical measurements were performed by an Autolab PGSTAT 302N apparatus. Cyclic voltammetric (CV) profiles were obtained with a three-electrode electrochemical system cell. Sulfuric acid 0.5 mol L^{-1} was used as supporting electrolyte, Hydrogen Electrode as reference (RHE), a platinum plate as counter-electrode and an ultrathin carbon vitreous layer previously polished as working electrode. For the working electrode preparation, an aliquot of ultrasonicated catalytic ink (10 μL) containing water (0.9 mL), isopropyl alcohol (0.1 mL), Nafion solution (5% – 20 μL) and catalytic powder (1 mg $mL^{-1}{}_{ink}$) was dropped on the tip of the vitreous carbon and dried. After nitrogen gas bubbled into H_2SO_4 solution for 30 min, CVs were recorded at 50 mV s^{-1} at ambient temperature, in a range of 0.05–0.8 V. Electro-oxidation measurements with methanol and ethanol (1 mol L^{-1}) were evaluated by CV in a potential range of 0.05–1 V, in order to avoid atomic rearrangement. For CO-stripping experiment, the working electrode was polarized at 0.25 V and carbon monoxide was bubbled during 15 min into electrolyte, followed by nitrogen gas for 30 min. For normalization purposes, electrochemical active surface area from CO stripping ($ECSA_{CO}$) was calculated following eq. (1):

$$ESCA_{CO} = \frac{Q_{CO}}{[Pt] q^0_{CO}} \quad (1)$$

where Q_{CO} is the CO oxidation charge, considering the electrical double layer contribution; *[Pt]* is the platinum loading and q^0_{CO} is the charge required to oxidize a CO monolayer adsorbed over platinum (420 μC cm^{-2}). To calculate the electrochemical active surface area (ECSA) based on the so called hydrogen adsorption/desorption region, eq. (1) was slightly adapted, changing Q_{CO} to Q_H (hydrogen desorption charge from 0.05 to 0.4 V, also considering the double layer contribution) and q^0_{CO} to q^0_H (desorption charge of a hydrogen monolayer on Pt – 210 μC cm^{-2}). The calculated ECSA for Pt/C was 46.7 m^2 g^{-1}_{Pt}, while Pt/C-(100) exhibited a value 38% smaller than the polycrystalline catalyst.

Fuel cell electrical performance

For MEAs (Membrane Electrode Assembly) preparation, synthesized Pt/C electrocatalysts were evaluated as anodes while commercial Pt/C (purchased from BASF, lot# F0381022) was chosen to cathodic side (both electrodes were loaded with 0.6 mg_{Pt} cm^{-2}). The 5 cm^2 electrodes were hot pressed to a pretreated Nafion® 115 membrane (Dupont) electrolyte at 125 °C for 10 min. All prepared MEAs were inserted in a unitary cell, operating at 80 °C, fueled with H_2/H_2CO gases (1000 ppm–300 mL min^{-1}) on the anode and O_2 on the cathodic side (200 mL min^{-1}). No backpressure was employed on the cathodic side to collect polarization curves.

Results and discussion

Fig. 1 shows TEM micrographs and XRD patterns of one-pot synthesized electrocatalysts from the reduction of a platinum salt by ethylene glycol on the carbon black support. Fig. 1a reveals well-dispersed spherical shaped Pt (Pt/C polycrystalline) nanoparticles prepared in the absence of the shape-directing agent, with an average particle size at 4 nm. On the other hand, in the presence of KBr, Fig. 1b evidences the preferential formation of Pt cubic nanoparticles (Pt/C-(100)) (average particle size at 8 nm). Fig. 1c exhibits in detail a cubic PtNP, where it is possible to observe the atomic lattice fringes. The measured interplanar distance from Fig. 1c is 1.99 Å and it corresponds to $d_{(200)}$ enclosed facets, which are expected for cubical morphology [6,33]. It is known that bromide can adsorb on Pt(100) domains [38]. Based on this fact, the novel synthesis route employed in this work was developed recently by Antoniassi *et al.* [37] resulting in a direct one-pot synthesis method promoted by KBr, which prevents the growth of Pt nanoparticles in the <100> direction. This environmentally friendly approach does not require post-

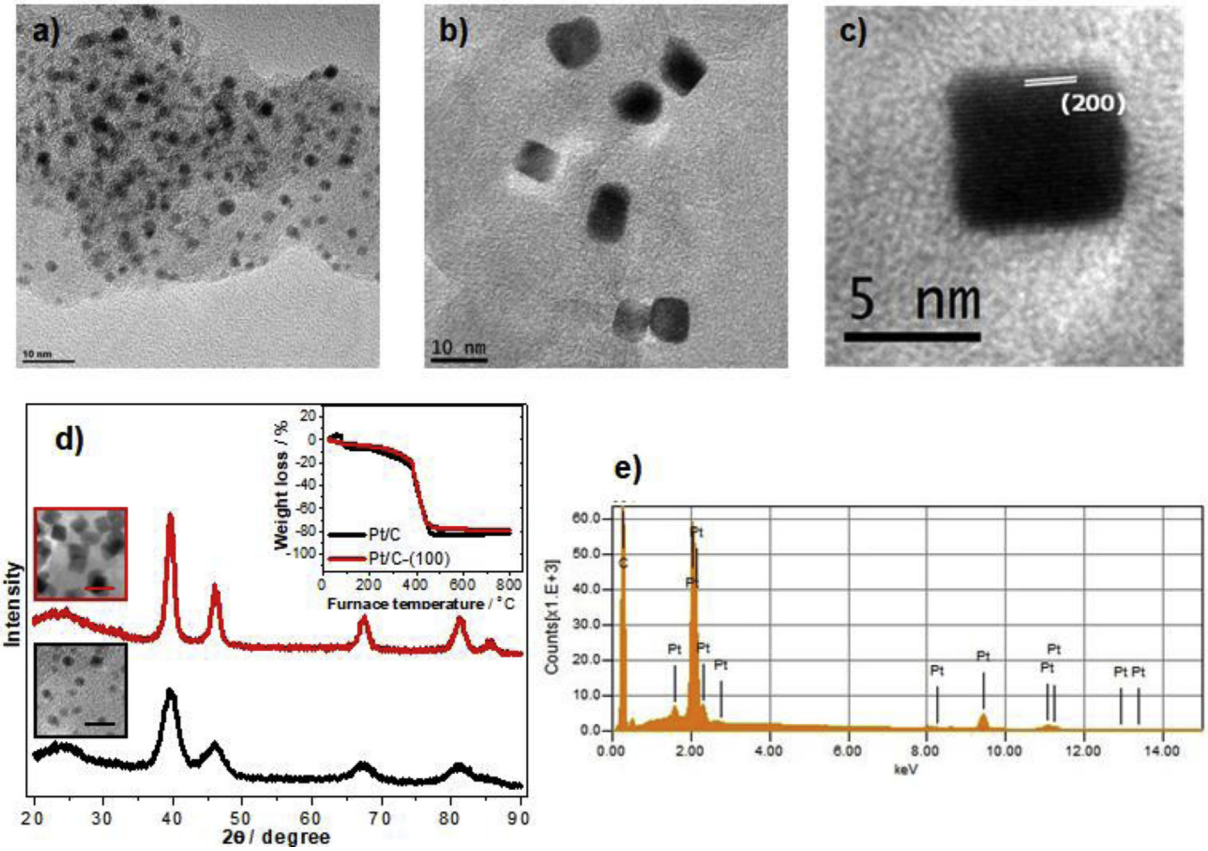

Fig. 1 – a) TEM images of Pt/C, b) Pt/C-(100), c) HR-TEM image of cubic Pt/C-(100) and d) XRD patterns (TEM bar corresponding to 10 nm) and TGA analysis in graph inset and e) EDS spectra of Pt/C-(100).

synthesis purification treatments, given that it is able to produce platinum nanoparticles with preferential Pt(100) orientation without the need for environmentally unfriendly stabilizing agents, e.g. PVP, which are known to interact strongly with the metal surface and to require rather complicated and undesirable post-synthesis purification routines [39–41]. Through this novel method, after the reduction of H_2PtCl_6 precursor, platinum nanoparticles surface is completely purified with a simple water-washing process, removing the adsorbed ions. Thus, (100)-terminated PtNPs are achieved at the final of the synthesis.

Fig. 1d shows XRD patterns of the Pt/C polycrystalline and the Pt/C-(100). Both diffractograms exhibited five peaks at 39°, 46°, 67°, 81°, 86° assigned to (111), (200), (220), (311) and (222) referent to the Pt face-centered cubic structure (Pt-FCC) [21,33]. A broad peak found at $2\theta \approx 25°$ is related to the hexagonal structure of the carbon black utilized as catalyst support [37,42]. There was no evidence for KBr presence on both the diffractograms. It is interesting to note that the ratio between $Pt_{(111)}/Pt_{(200)}$ intensities from the XRD data in Fig. 1d is 2.88 for the Pt/C polycrystalline and 1.47 for the Pt/C-(100), which also indicates that the latter material is more abundant in Pt(100) facets. From data in Fig. 1d it is further possible to observe that Pt-FCC peaks of Pt/C polycrystalline are broader than Pt/C-(100), suggesting that Pt/C polycrystalline nanoparticles are smaller than Pt/C-(100), which is in accordance with TEM micrographs of Fig. 1b (average particle size at about 8 nm). To establish the metal load in both materials, TGA experiment was conducted up to a temperature of 800 °C. As can be observed from the inset in Fig. 1d, at 500 °C carbon is completely burned off leaving only the mass referent to the platinum content, which was close to 20% in mass in both catalysts, in suitable agreement with the desired platinum content. Fig. 1e shows EDS spectra data of Pt/C-(100). Based on the elementary analysis, only platinum and carbon signals were verified. There was no bromide on the obtained material, indicating that the bromine employed as directing agent was completely removed from nanoparticles surface through the simple DI water washing process.

Considering that the cubic Pt/C-(100) catalyst is richer in Pt(100) facets, distinct cyclic voltammetry profiles would be expected for this material compared to that of the Pt/C polycrystalline catalyst. Based on investigations of the hydrogen adsorption/desorption region on Pt monocrystals and polyoriented nanoparticles in acid media [43,44], a peak centered approximately at 0.125 V vs RHE corresponds to the process on Pt(110) sites. In addition, two more peaks related to the hydrogen desorption on Pt(100) sites are found close to 0.27 and 0.35 V (related to Pt(100) stepped sites on Pt(111) terraces and bidimensional Pt(100) terraces, respectively) [43,44]. Based on these distinct features, cyclic voltammograms were recorded in nitrogen saturated electrolyte for both Pt/C-(100) and Pt/C polycrystalline. Fig. 2a exhibits these voltammograms, which are typical for Pt/C [44], though it evidences that

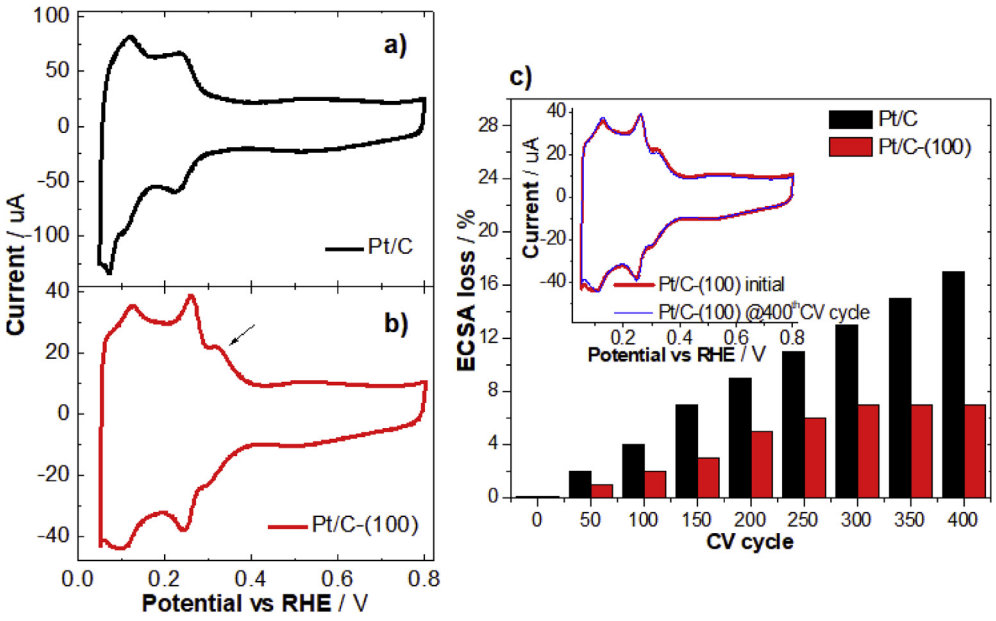

Fig. 2 – Cyclic voltammograms recorded in 0.5 mol L^{-1} H_2SO_4 at 50 mV s^{-1}, a) Pt/C polycrystalline, b) Pt/C-(100) and c) ECSA loss in 400 CV cycles.

the hydrogen desorption charge from the Pt(100) facet is considerably pronounced in the cubic Pt/C-(100) versus the Pt/C polycrystalline catalyst. In agreement with TEM and XRD data, the ratio between the hydrogen desorption peaks from Pt(110) and Pt(100) faces on the voltammograms in Fig. 2a and b evidences that the Pt/C-(100) catalyst is preferentially formed by (100) facets (cubic Pt nanoparticles). Considering the hydrogen desorption peaks at 0.125 V vs RHE for Pt(110) and at 0.250 V vs RHE for Pt(100), the ratio Pt(110)/Pt(100) for the Pt/C-(100) is 0.95 and for the Pt/C polycrystalline this is 1.18. Furthermore, a third peak (indicated by the black arrow) at around 0.350 V vs RHE, also assigned to Pt(100) facets [44], became notable in the voltammogram of the Pt/C-(100) catalyst (Fig. 2b), which is absent in Pt/C polycrystalline profile (Fig. 2a).

As aforementioned, low-temperature fuel cells are one application of Pt/C-based materials. These devices require most commonly nanostructured platinum (Pt/C) catalyst to achieve acceptable reaction rates on both anode and cathode electrodes, however, it is still unable to meet long term durability targets [45]. Therefore, a comparison was performed in terms of durability of the cubic Pt/C-(100) versus the polycrystalline Pt/C material. The catalyst stability was evaluated by extensive potential cycling from 0.05 to 0.8 V (Fig. 2c). It was observed an electrochemically active surface area (ECSA) loss of approximately 16% for Pt/C after the 400 potential cycles, where this ECSA loss clearly, and approximately linearly, increases with the number of cycles, in agreement with other reports in the literature [46]. In contrast, for the cubic Pt/C-(100), it is observed from data in Fig. 2c that the ECSA loss reached an equilibrium from the ~300th cycle and on, losing less than 7% of the initial ECSA value, which seems extremely promising in terms of known stability targets for platinum metal group catalysts [45]. It might also indicates no atomic rearrangements, as suggested by the Pt(110)/Pt(100) ratio after the 400 potential cycles (less than 2% higher than the initial data), so that the cubic PtNPs morphology seems to be persevered in the final voltammogram profile (inset in Fig. 2c). This further points to the resilience and the promise of this type of shape-controlled material towards addressing durability issues in fuel cells, among other energy conversion devices.

Oxidation of small organic molecules would be an important application for cubic platinum nanoparticles given that the Pt(100) facet is more active towards such reactions [6,27]. Therefore, a comparison was carried out in order to estimate the electrocatalytic activity of the preferentially cubic Pt/C-(100) in comparison to that of the polycrystalline Pt/C catalysts towards the oxidation of methanol, ethanol and carbon monoxide, where the latter is generally accepted to limit the reaction rate for the complete oxidation of the former molecules up to carbon dioxide [47,48].

CO electrooxidation

Data in Fig. 3a compares the catalytic activity of the catalysts Pt/C-(100) and Pt/C polycrystalline for the electrooxidation of a one-layer adsorbed carbon monoxide through the known CO-stripping technique. Since platinum has a structural-sensitive interaction with CO, this molecule has been used as a molecular probe to study Pt surface structural changes [49–51]. As can be seen in Fig. 3a, the voltammetric profiles for the electrooxidation of CO are clearly different for the preferentially cubic Pt/C-(100) in comparison to that on the polycrystalline Pt/C nanomaterial. The voltammogram for the electrooxidation of CO on the polycrystalline Pt/C presents only one peak centered at about 0.86 V vs RHE, which is commonly seen in the literature [49,51,52]. However, three peaks ~0.75 V (I), ~0.79 V (II) and ~0.86 V (III) vs RHE are clearly observed at lower potentials in Fig. 3a for the same oxidative

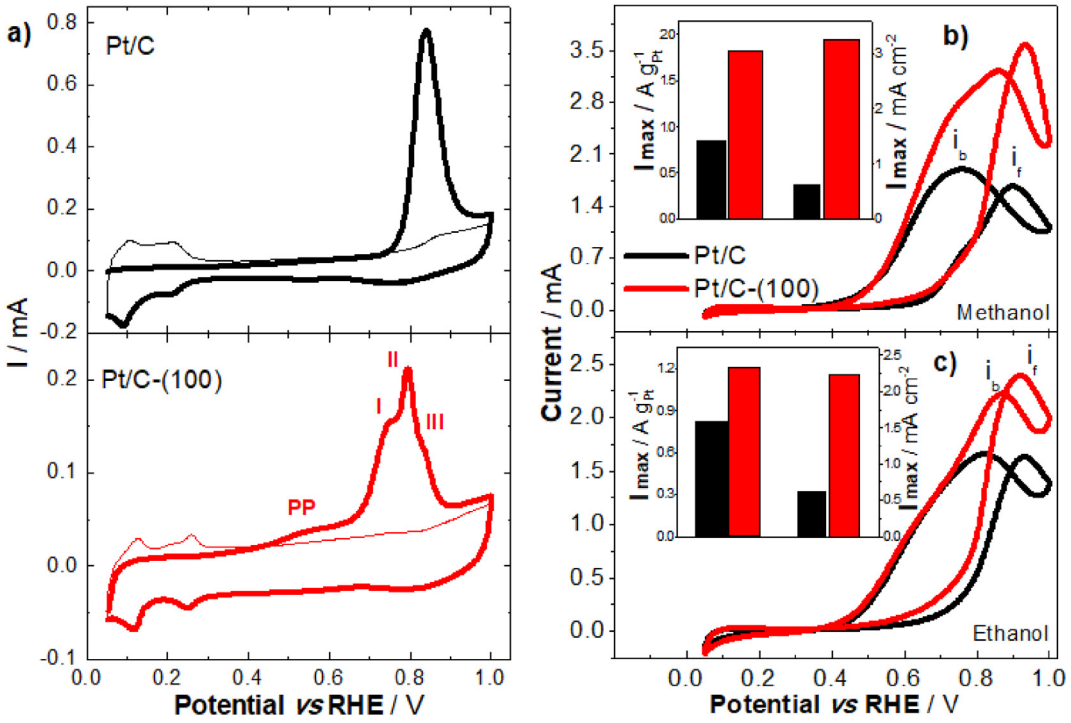

Fig. 3 – Cyclic voltammograms. CO-stripping experiments recorded at 50 mV s^{-1} in 0.5 mol L^{-1} H_2SO_4, b) 1 mol L^{-1} of methanol in 0.5 mol L^{-1} H_2SO_4 recorded at 50 mV s^{-1}, c) 1 mol L^{-1} of ethanol in 0.5 mol L^{-1} H_2SO_4 recorded at 50 mV s^{-1}. The graph insets correspond to the maximum current density normalized per $ECSA_{CO}$ and Pt load.

reaction on the preferentially cubic Pt/C-(100) catalyst. As already mentioned, the electrooxidation of CO is a structure-sensitive reaction, and modifications in the characteristics of surface sites promote different CO-stripping profiles, usually leading to peak splitting, which are dependent on the CO adsorption sites [53]. The multiple peaks towards CO electro-oxidation could be originated on different facets, such terraces (100), (111) and (110) sites [54]. Therefore, the splitting in CO oxidation peaks is relative to the surface site distribution. It is reported that CO oxidation on Pt terrace surface occurs at lower overpotentials, while that near the edge and/or corner sites appears at more positive potential values (higher overpotentials) [53]. Guerin et al. [55] reported on similar observations. The peak at most negative potentials was ascribe to CO oxidation on terraces predominant on the larger materials, while the most positive peak is related to the edges sites in smaller particles. In the present study, the splitting of CO peaks might be associated to increased terrace surfaces contained in the cubes of Pt/C-(100), in contrast to the irregular surface of spherical shaped polycrystalline Pt/C nanoparticles. In acidic media, it is well-know that defect sites (steps, kinks and edge sites) possess an enhanced activity towards CO electrooxidation in platinum electrodes. They play an important dual role (at least in alkaline media) on CO oxidation mechanism: CO adsorbed on bottom side of the step site is more reactive, while the CO located on the top of the step is less active, reacting with OH activated on the Pt(100) terrace [56]. Koper et al. [57] observed that CO adsorbed both near the stepped sites and on the terrace of Pt(100) surfaces could be easily oxidized to CO_2 at the step sites. This fact suggests that the obtained cubic Pt nanoparticles is not exclusively built by flat Pt(100) surfaces, though it also contains amounts of stepped sites and/or other defects. On the other hand, the activity of CO oxidation on Pt(111) terraces is negligible, thus forcing a rapid CO diffusion to the step sites in order to oxidize. Furthermore, defects such as edge and kink sites (with lower coordinating number than step sites) seem to be more active in alkaline media [58,59]. García et al. [60], in a similar way than acidic media, observed that the step sites of Pt(100) are more active than those of Pt(111) towards the oxidation of CO.

According to Urchaga et al. and Brimaud et al. [49,61,62], a peak at around 0.76 V (I) vs RHE may be related to adsorbed CO on (111) terraces, which migrates towards active sites and/or on long range (100) bi-dimensional surface domains, while the peak at ~ 0.79 V (II) vs RHE might be related to the short range (100) surface domains [49]. These peaks are clearly seen in Fig. 3a for the electrooxidation of CO on the preferentially cubic Pt/C-(100) catalyst, though not on the polycrystalline Pt/C material. Furthermore, a pre-peak (PP) is observed at about 0.4–0.6 V on the Pt/C-(100). The origin of this pre-peak has been extensively debated in the literature in acid and alkaline media. Brimaud et al. [61] was categorical to conclude that the pre-peak is related to the presence of (100) and (111) terraces and its shape changes with terraces symmetry. For Pastor et al. [63] the reason of the PP is related to the presence of "special sites" – such as low-coordinated atoms – which could easily dissociate the water molecule. Moreover, García et al. [54] reported that the charge observed in the region below the PP is associated to CO oxidation on border, step,

edge or kink sites that presumably present (100) and (110) facets. Bartlett et al. [64] attributed the pre-peak (pre-wave) to the concave nature of porous Pt material, which contains a significant number of Pt sites located at low index facets of concave surface meet. The pre-wave could be an indicative of facilitated CO stripping process involving OH adsorption. Coutanceau et al. [50] explained the PP feature in terms of weakly adsorbed CO for the electro-oxidation of CO on exclusively cubic shaped PtNPs (nanoparticles prepared with stabilizing agents). Incidentally, Solla-Gullón et al. [65] synthesized highly Pt(100) oriented nanoparticles by the water-in-oil method, using hydrazine and sodium borohydride. They presented a similar CO profile to the current work, containing both PP and peak splitting. Therefore, such characteristics in CO monolayer oxidation are closely linked to the nature of the surface sites. It is remarkable that a modification on the nanoparticles domain can promote notable changes on the CO-stripping feature. Considering the cited works, the presence of the PP may involve not only the flat surfaces but crystalline specific defects on the structure of the Pt-(100) material. Nevertheless, this pre-peak is greatly desirable, as it would potentially result in lower overpotentials for the oxidation of methanol, ethanol and further for polymer electrolyte fuel cell (PEFCs) anodes fed with hydrogen streams contaminated with CO (e.g. from fuel reforming).

It is interesting to note that the ratio between Q_H to Q_{CO} in the CO-stripping experiments was below the theoretical 0.5 value. For Pt/C polycrystalline the calculated ratio was 0.44 and 0.32 for preferential oriented Pt/C-(100). Similar differences have also being reported by Friedrich and Henglein [66], and Maillard et al. [67]. According to these authors, despite of the uncertainty in the determination of Q_H on nanoparticles, a ratio between Q_H to Q_{CO} below the theoretical value indicates higher packing density of adsorbed CO on nanoparticles than in extended surfaces. This result suggests that a ratio below 0.5 is characteristic of nanometer-sized particles, however such fact requires further investigation.

Methanol and ethanol electrooxidation

Considering the desirable and interesting direct alcohol fuel cells (DAFCs), the electrocatalytic activity of both Pt/C-(100) and Pt/C polycrystalline was assessed towards the oxidation of methanol and ethanol, which voltammetric features are displayed in Fig. 3b and c, respectively.

The electrooxidation of methanol starts at about 0.4 V *vs* RHE on the preferentially cubic Pt/C-(100) catalyst, while on Pt/C it starts at about 0.51 V *vs* RHE, which indicates a higher catalytic activity of the former in comparison to the polycrystalline material. Moreover, the maximum current density in the forward scan normalized per platinum load was 1.81 A g_{Pt}^{-1} for the preferentially cubic Pt/C-(100) catalyst, which value is 46% higher than that obtained for the polycrystalline Pt/C. The superior maximum current density behaviour of Pt/C-(100) was also observed in terms of electrochemical active surface area ($ECSA_{CO}$), yielding 3.26 A cm^{-2} for the Pt/C-(100) compared to only 0.63 A cm^{-2} for the Pt/C catalyst. This normalization analysis clearly evidences that the preferentially cubic catalyst presents an exposed surface that is five times more active than the traditional Pt/C polycrystalline catalyst. Similar results were reported by Housmans et al. [11] showing that the reactivity for the methanol oxidation reaction is highest on the Pt(100) domain in comparison to the other platinum basal planes, and that it proceeds predominantly via the indirect oxidation pathway through adsorbed carbon monoxide.

Voltammograms in Fig. 3c compare the catalytic activity of both the Pt/C-(100) and Pt/C catalysts towards the oxidation of ethanol in acidic media. At 0.05 V, a competitive adsorption between hydrogen/ethanol is expected, however the alcohol cannot adsorb at this condition. As the potential values turn more positive in the forward scan, H_{ads} desorbs and ethanol adsorption/electrooxidation takes place on the available platinum sites [15,63]. The onset potential for the reaction on the preferentially cubic Pt/C-(100) catalyst is at about 0.44 V vs RHE, which is lower than that on the polycrystalline Pt/C material (0.56 V vs RHE). Although the mechanism for the electrooxidation of ethanol is complex (involving several intermediates, which can be concomitantly formed), Pastor et al. [15,63] reported on insights about the EOR through an online mass spectroscopy approach. They found methane as the principal product of ethanol electro-oxidation in potential values until at 0.4 V for acidic media (no signals from the other products were observed at potentials close 0.4 V). As opposed to acetaldehyde or acetic acid formations, methane requires the C–C bond cleavage, which could be an indication that the Pt/C-(100) catalyst favours the C–C cleavage in lower potentials compared to the polycrystalline material. Bounded C–C intermediates are obtained at up to 0.4 V, e.g. adsorbed acetaldehyde oxidation to acetic acid and other ethanol fragments to CO_2 occur at values > 0.6 V. At upper potentials till 0.8 V, CO_2 seems to fall to zero and acetaldehyde contribution decreases, once PtO_X – is formed at this stage – inhibiting the adsorption of alcohol molecules. During the backward scan, platinum oxide is reduced, then, ethanol (and other products) re-adsorbs in order to react again. However, no carbon dioxide is produced in this scan [15,63].

Data in Fig. 3b and c exhibits that the maximum current density values, in the forward scan, for the electrooxidation of methanol and ethanol were 1.21 A g_{Pt}^{-1} and 2.24 A cm^{-2} (normalized per Pt load and $ECSA_{CO}$, respectively). These values are 68% and 28% higher than those obtained on Pt/C, as depicted in the same data. This indicates that Pt/C-(100) has a superior catalytic activity towards the oxidation of both methanol and ethanol compared to Pt/C polycrystalline.

According to previous studies [6,68–71], the ratio between the forward (i_f) and backward (i_b) voltammetric current peaks, for the oxidation of alcohols (Fig. 3b and c), illustrates the intermediate carbonaceous species adsorbed on the catalyst surface. These species are generated in the forward scan and oxidized/desorbed in the backward scan. This results that a low i_f/i_b ratio indicates excessive accumulation of carbonaceous species on the catalyst surface, while a high i_f/i_b ratio suggests less accumulation of residues on the material surface. Therefore, a high i_f/i_b ratio would be an indicative of an improved catalytic activity, while a low i_f/i_b ratio would suggest a catalyst sensitive to undergo poisoning by the intermediates/by-products of the oxidation of the alcohol. In the present study, the measured i_f/i_b ratios for the oxidation of methanol were 1.13 for Pt/C-(100) and 0.87 for Pt/

C, and for the oxidation of ethanol the values were 1.10 for Pt/C-(100) and 0.96 for the polycrystalline Pt/C (Fig. 3b and c). The higher i_f/i_b values measured for the preferentially cubic Pt/C-(100) nanoparticles in comparison to those measured for the polycrystalline Pt/C suggest fewer intermediates/by-products left adsorbed on the surface of the Pt/C-(100) and a higher amount adsorbed on the polycrystalline Pt/C nanoparticles. Han et al. [6] also performed experiments using Pt/C nanocubes (synthesized with PVP as stabilizing agent) and Pt/C polycrystalline for the electrooxidation of alcohols and measured higher i_f/i_b ratios for cubic shaped particles. The authors attributed this peak ratio differences to an efficient removal of incompletely oxidized carbonaceous species on the preferentially cubic Pt/C catalyst, where these by-products were attributed to be mostly associated with linearly bonded Pt=C=O. Furthermore, data in Figs. 3a and 4 evidences that the oxidation of carbon monoxide on cubic nanoparticles occurs at lower overpotentials in comparison to that on spherical shaped nanoparticles, which would potentially support the observed higher catalytic activity of cubic Pt/C catalysts for oxidizing both methanol and ethanol (Fig. 3b and c). Additionally, some studies have shown that Pt(100) preferentially oriented is more effective in breaking the C–C bond, yielding adsorbed CO, which is an obligatory intermediate for CO_2 formation [27,33]. In fact, through direct ethanol fuel cell experiments, Antoniassi et al. [37] has measured the product distribution from the oxidation of ethanol on some catalysts and observed that carbon dioxide is not formed on polycrystalline platinum nanoparticles, while it is formed at a considerable percentage on cubic platinum nanoparticles (i.e. 7.4% in mols of the total products). These results point to the promising development of shape-controlled electrocatalysts towards promoting practically valued liquid-fuelled fuel cells [72].

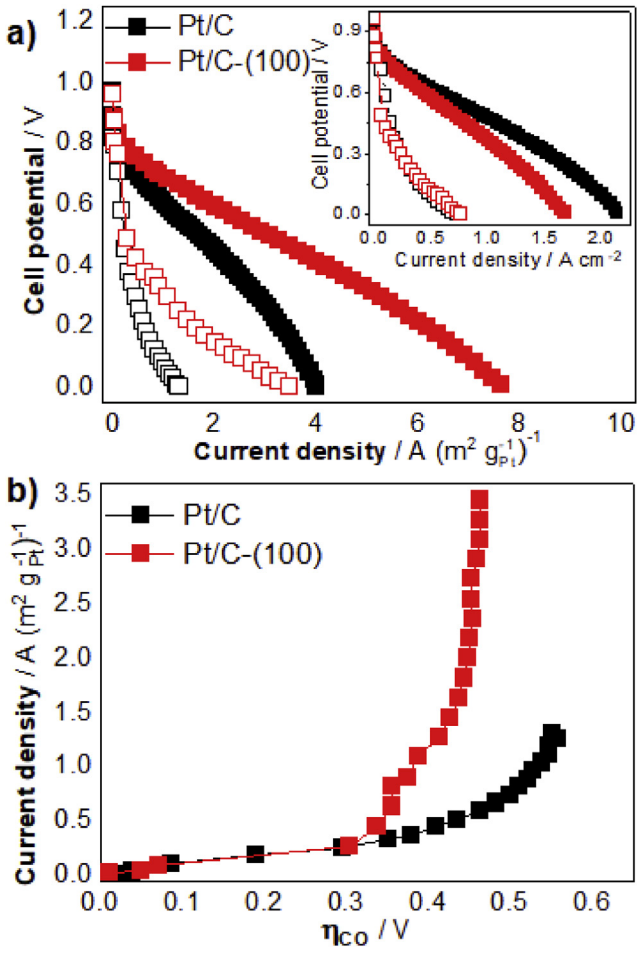

Fig. 4 – a) Single cell performance plots for a Pt/C and Pt/C-(100) electrodes with H_2 (solid squares) and H_2–CO (1000 ppm – open squares) normalized per $ECSA_{CO}$ and the inset normalized by Pt load, b) overpotential (η_{CO}) as a function of the measured current density b).

Fuel cell measurements

Further testing the catalytic activity of shape-controlled platinum nanoparticles, Fig. 4a exhibits PEFC polarization curves (V *vs* j – normalized per $ECSA_{CO}$ and Pt load, as electrode area) in a single polymer electrolyte fuel cell device fed with pure hydrogen and with a hydrogen CO mixture at relatively low, though practical, operating temperature. PEFCs having the preferentially cubic Pt/C-(100) or the polycrystalline Pt/C as anode catalyst exhibit an open circuit voltage at approximately 0.97 V in H_2/O_2 or in H_2-CO/O_2 configurations. However, the measured PEFC maximum specific current density obtained with Pt/C-(100) as anode catalyst was 7.6 A $(m^{-2}\,g^{-1}{}_{Pt})^{-1}$, which is 48% higher than that obtained with the Pt/C in H_2/O_2 fuelled PEFC. More importantly, when the PEFC anode is supplied with a H_2-CO steam, the Pt/C-(100) material exhibited a higher performance upon appropriately normalizing the measured current density by the electrochemical active Pt surface area, which strongly suggests, as measured in Fig. 3a, a higher catalytic activity of the cubic catalyst towards oxidizing CO at lower overpotentials in comparison to the polycrystalline Pt/C. This tolerance to CO poisoning on the shape-controlled platinum catalyst is further evidenced upon comparing the single cell anode overpotential (η_{CO}) as a function of the measure PEFC current density. Fig. 4b clearly evidences, as in Fig. 3a, that CO is oxidized at lower potential values on the Pt/C-(100) compared to Pt/C. At the PEFC temperature conditions (80 °C), the gap of potential between Pt/C-(100) and Pt/C observed in Fig. 4b is at about 0.18 V, in agreement with CO stripping tests performed at ambient temperature, which further suggests that the catalytic activity difference is primarily structural in nature. Further developments in this area could lead to the development of preferentially cubic Pt nanoparticles at desirable smaller diameters, which would potentially lead to materials directly applicable in practical devices.

Conclusions

Versatile shape controlled Pt nanoparticles were synthesized by an environmentally friendly one-pot synthesis method directly on the desired catalyst support material. Cubic-shaped Pt/C-(100) exhibited different hydrogen adsorption/desorption and CO-stripping voltammetry profiles compared to a Pt/C polycrystalline, which evidenced the dominant cubic

nature of the former nanomaterial as also evidenced by TEM and other physical characterization techniques. Pt/C polycrystalline showed only one peak for CO-stripping at 0.86 V. Pt/C-(100) exhibited three peaks at about 0.75–0.86 V and a pre-peak at 0.4 V, which could be associated to the not only to the presence of flat Pt(100) surface, but defects such border, step, kink and edge sites, yielding a particular nanoparticle surface in this electrocatalyst. Higher current densities were obtained from ethanol and methanol electrooxidation using Pt/C-(100) in comparison to Pt/C polycrystalline, which was in suitable agreement with the onset potential for the oxidation of CO on these catalysts. Additionally, the ratio between the forward (i_f) and backward (i_b) voltammetric current density peaks for the oxidation of these alcohols suggests that Pt/C-(100) is less affected by adsorbed intermediates from ethanol and methanol electrooxidation than Pt/C polycrystalline. Furthermore, the performance of a single polymer electrolyte fuel cell device fed with pure hydrogen and with a CO-contaminated hydrogen (1000 ppm) mixture was superior employing Pt/C-(100) anode than Pt/C polycrystalline, which further evidenced the practical potential of this material.

Acknowledgments

The authors thanks CNPq Proc. n° 310051/2012-6 and 443046/2014-0, FAPESP Proc. n° 2014/09087-4 and CAPES for financial support. R.M.A would like to thank the Comissão Nacional de Energia Nuclear (CNEN) to support the actual project. T.L. would also like to thank the Sao Paulo Research Foundation under projects 14/22130-6 and 17/15304-6 for T.L.'s Young Investigator Award. Authors also acknowledge the support of the RCGI Research Centre for Gas Innovation, sponsored by FAPESP (2014/50279-4) and Shell. Use of TEM facilities (JEOL JEM 2100F) of LNNano-CNPEM is greatly acknowledged.

REFERENCES

[1] Chen C-Y, Lai W-H, Yan W-M, Chen C-C, Hsu S-W. Effects of nitrogen and carbon monoxide concentrations on performance of proton exchange membrane fuel cells with Pt–Ru anodic catalyst. J Power Sources 2013;243:138–46.
[2] Wang W, Wang W, Chen S. The effects of hydrogen dilution, carbon monoxide poisoning for a Pt–Ru anode in a proton exchange membrane fuel cell. Int J Hydrogen Energy 2016;41:20680–92.
[3] Akhairi MAF, Kamarudin SK. Catalysts in direct ethanol fuel cell (DEFC): an overview. Int J Hydrogen Energy 2016;41:4214–28.
[4] Silva JCM, De Souza RFB, Romano MA, D'Villa-Silva M, Calegaro ML, Hammer P, et al. PtSnIr/C anode electrocatalysts: promoting effect in direct ethanol fuel cells. J Braz Chem Soc 2012;23:1146–53.
[5] Chu Y-H, Ahn S-W, Kim D-Y, Kim H-J, Shul Y-G, Han H. Combinatorial investigation of Pt-Ru-M as anode electrocatalyst for direct methanol fuel cell. Catal Today 2006;111:176–81.
[6] Han S-B, Song Y-J, Lee J-M, Kim J-Y, Park K-W. Platinum nanocube catalysts for methanol and ethanol electrooxidation. Electrochem Commun 2008;10:1044–7.
[7] Lee SJ, Mukerjee S, Ticianelli EA, McBreen J. Electrocatalysis of CO tolerance in hydrogen oxidation reaction in PEM fuel cells. Electrochim Acta 1999;44:3283–93.
[8] Camara GA, Ticianelli EA, Mukerjee S, Lee SJ, McBreen J. The CO poisoning mechanism of the hydrogen oxidation reaction in proton exchange membrane fuel cells. J Electrochem Soc 2002;149:A748–53.
[9] Mondal S, Malik S. Easy synthesis approach of Pt-nanoparticles on polyaniline surface: an efficient electro-catalyst for methanol oxidation reaction. J Power Sources 2016;328:271–9.
[10] Grozovski V, Climent V, Herrero E, Feliu JM. The role of the surface structure in the oxidation mechanism of methanol. J Electroanal Chem 2011;662:43–51.
[11] Housmans THM, Wonders AH, Koper MTM. Structure sensitivity of methanol electrooxidation pathways on Platinum: an on-line electrochemical mass spectrometry study. J Phys Chem B 2006;110:10021–31.
[12] da Silva SG, Assumpção MHMT, de Souza RFB, Buzzo GS, Spinacé EV, Neto AO, et al. Electrochemical and fuel cell evaluation of PtIr/C electrocatalysts for ethanol electrooxidation in alkaline medium. Electrocatalysis 2014;5:438–44.
[13] Switzer EE, Olson TS, Datye AK, Atanassov P, Hibbs MR, Cornelius CJ. Templated Pt-Sn electrocatalysts for ethanol, methanol and CO oxidation in alkaline media. Electrochim Acta 2009;54:989–95.
[14] Gao H, Liao S, Liang Z, Liang H, Luo F. Anodic oxidation of ethanol on core-shell structured Ru@PtPd/C catalyst in alkaline media. J Power Sources 2011;196:6138–43.
[15] Guillén-Villafuerte O, García G, Arévalo MC, Rodríguez JL, Pastor E. New insights on the electrochemical oxidation of ethanol on carbon-supported Pt electrode by a novel electrochemical mass spectrometry configuration. Electrochem Commun 2016;63:48–51.
[16] Busó-Rogero C, Brimaud S, Solla-Gullon J, Vidal-Iglesias FJ, Herrero E, Behm RJ, et al. Ethanol oxidation on shape-controlled platinum nanoparticles at different pHs: a combined in situ IR spectroscopy and online mass spectrometry study. J Electroanal Chem 2016;763:116–24.
[17] Sun C-L, Tang J-S, Brazeau N, Wu J-J, Ntais S, Yin C-W, et al. Particle size effects of sulfonated graphene supported Pt nanoparticles on ethanol electrooxidation. Electrochim Acta 2015;162:282–9.
[18] Crisafulli R, Antoniassi RM, Oliveira Neto A, Spinacé EV. Acid-treated PtSn/C and PtSnCu/C electrocatalysts for ethanol electro-oxidation. Int J Hydrogen Energy 2014;39:5671–7.
[19] Nakagawa N, Ito Y, Tsujiguchi T, Ishitobi H. Improved reaction kinetics and selectivity by the TiO2-embedded carbon nanofiber support for electro-oxidation of ethanol on PtRu nanoparticles. J Power Sources 2014;248:330–6.
[20] García G, Tsiouvaras N, Pastor E, Peña MA, Fierro JLG, Martínez-Huerta MV. Ethanol oxidation on PtRuMo/C catalysts: in situ FTIR spectroscopy and DEMS studies. Int J Hydrogen Energy 2012;37:7131–40.
[21] Antoniassi RM, Oliveira Neto A, Linardi M, Spinacé EV. The effect of acetaldehyde and acetic acid on the direct ethanol fuel cell performance using PtSnO2/C electrocatalysts. Int J Hydrogen Energy 2013;38:12069–77.
[22] Rizo R, Sebastián D, Lázaro MJ, Pastor E. On the design of Pt-Sn efficient catalyst for carbon monoxide and ethanol oxidation in acid and alkaline media. Appl Catal B Environ 2017;200:246–54.
[23] Thepkaew J, Therdthianwong S, Therdthianwong A, Kucernak A, Wongyao N. Promotional roles of Ru and Sn in mesoporous PtRu and PtRuSn catalysts toward ethanol electrooxidation. Int J Hydrogen Energy 2013;38:9454–63.

[24] Zhao Y, Zhou Y, O'Hayre R, Shao Z. Electrocatalytic oxidation of methanol on Pt catalyst supported on nitrogen-doped graphene induced by hydrazine reduction. J Phys Chem Solids 2013;74:1608–14.
[25] Spindola RF, Zanin H, Macena CS, Contin A, de Cássia Silva Luz R, Damos FS. Evaluation of a novel composite based on functionalized multi-walled carbon nanotube and iron phthalocyanine for electroanalytical determination of isoniazid. J Solid State Electrochem 2017;21:1089–99.
[26] Xiong B, Zhou Y, Zhao Y, Wang J, Chen X, O'Hayre R, et al. The use of nitrogen-doped graphene supporting Pt nanoparticles as a catalyst for methanol electrocatalytic oxidation. Carbon 2013;52:181–92.
[27] Buso-Rogero C, Grozovski V, Vidal-Iglesias FJ, Solla-Gullon J, Herrero E, Feliu JM. Surface structure and anion effects in the oxidation of ethanol on platinum nanoparticles. J Mater Chem A 2013;1:7068–76.
[28] Nakamura M, Hanioka Y, Ouchida W, Yamada M, Hoshi N. Estimation of surface structure and carbon monoxide oxidation site of shape-controlled Pt nanoparticles. ChemPhysChem 2009;10:2719–24.
[29] Busó-Rogero C, Herrero E, Feliu JM. Ethanol oxidation on Pt single-crystal electrodes: surface-structure effects in alkaline medium. ChemPhysChem 2014;15:2019–28.
[30] Colmati F, Tremiliosi-Filho G, Gonzalez ER, Berna A, Herrero E, Feliu JM. Surface structure effects on the electrochemical oxidation of ethanol on platinum single crystal electrodes. Faraday Discuss 2009;140:379–97.
[31] Colmati F, Tremiliosi-Filho G, Gonzalez ER, Berna A, Herrero E, Feliu JM. The role of the steps in the cleavage of the C-C bond during ethanol oxidation on platinum electrodes. Phys Chem Chem Phys 2009;11:9114–23.
[32] Souza-Garcia J, Herrero E, Feliu JM. Breaking the C–C bond in the ethanol oxidation reaction on platinum electrodes: effect of steps and ruthenium adatoms. ChemPhysChem 2010;11:1391–4.
[33] Figueiredo MC, Solla-Gullón J, Vidal-Iglesias FJ, Nisula M, Feliu JM, Kallio T. Carbon-supported shape-controlled Pt nanoparticle electrocatalysts for direct alcohol fuel cells. Electrochem Commun 2015;55:47–50.
[34] Antoniassi RM, Silva JCM, Oliveira Neto A, Spinacé EV. Synthesis of Pt+SnO2/C electrocatalysts containing Pt nanoparticles with preferential (100) orientation for direct ethanol fuel cell. Appl Catal B Environ 2017;218:91–100.
[35] Naresh N, Wasim FGS, Ladewig BP, Neergat M. Removal of surfactant and capping agent from Pd nanocubes (Pd-NCs) using tert-butylamine: its effect on electrochemical characteristics. J Mater Chem A 2013;1:8553–9.
[36] Huang MH, Chiu C-Y. Achieving polyhedral nanocrystal growth with systematic shape control. J Mater Chem A 2013;1:8081–92.
[37] Antoniassi RM, Otubo L, Vaz JM, Oliveira Neto A, Spinacé EV. Synthesis of Pt nanoparticles with preferential (1 0 0) orientation directly on the carbon support for Direct Ethanol Fuel Cell. J Catal 2016;342:67–74.
[38] Orts JM, Gómez R, Feliu JM, Aldaz A, Clavilier J. Voltammetry, charge displacement experiments, and scanning tunneling microscopy of the Pt(100)–Br system. Langmuir 1997;13:3016–23.
[39] Krier JM, Michalak WD, Baker LR, An K, Komvopoulos K, Somorjai GA. Sum frequency generation vibrational spectroscopy of colloidal platinum nanoparticle catalysts: disordering versus removal of organic capping. J Phys Chem C 2012;116:17540–6.
[40] Monzó J, Koper MTM, Rodriguez P. Removing polyvinylpyrrolidone from catalytic Pt nanoparticles without modification of superficial order. ChemPhysChem 2012;13:709–15.
[41] Fernández PS, Ferreira DS, Martins CA, Troiani HE, Camara GA, Martins ME. Platinum nanoparticles produced by EG/PVP method: the effect of cleaning on the electro-oxidation of glycerol. Electrochim Acta 2013;98:25–31.
[42] Silva JCM, Anea B, De Souza RFB, Assumpcao MHMT, Calegaro ML, Neto AO, et al. Ethanol oxidation reaction on IrPtSn/C electrocatalysts with low Pt content. J Braz Chem Soc 2013;24:1553–60.
[43] Vidal-Iglesias FJ, Arán-Ais RM, Solla-Gullón J, Herrero E, Feliu JM. Electrochemical characterization of shape-controlled Pt nanoparticles in different supporting electrolytes. ACS Catal 2012;2:901–10.
[44] Martınez-Rodrıguez RA, Vidal-Iglesias FJ, Solla-Gullón J, Cabrera CR, Feliu JM. Synthesis of Pt nanoparticles in water-in-oil microemulsion: effect of HCl on their surface structure. J Am Chem Soc 2014;136:1280–3.
[45] Banham D, Ye S. Current status and future development of catalyst materials and catalyst layers for proton exchange membrane fuel cells: an industrial perspective. ACS Energy Lett 2017;2:629–38.
[46] Lim D-H, Choi D-H, Lee W-D, Lee H-I. A new synthesis of a highly dispersed and CO tolerant PtSn/C electrocatalyst for low-temperature fuel cell; its electrocatalytic activity and long-term durability. Appl Catalysis B Environ 2009;89:484–93.
[47] Gisbert R, García G, Koper MTM. Oxidation of carbon monoxide on poly-oriented and single-crystalline platinum electrodes over a wide range of pH. Electrochim Acta 2011;56:2443–9.
[48] Cuesta A, Couto A, Rincón A, Pérez MC, López-Cudero A, Gutiérrez C. Potential dependence of the saturation CO coverage of Pt electrodes: the origin of the pre-peak in CO-stripping voltammograms. Part 3: Pt(poly). J Electroanal Chem 2006;586:184–95.
[49] Urchaga P, Baranton S, Coutanceau C. Changes in CO chem oxidative stripping activity induced by reconstruction of Pt (1 1 1) and (1 0 0) surface nanodomains. Electrochim Acta 2013;92:438–45.
[50] Coutanceau C, Urchaga P, Baranton S. Diffusion of adsorbed CO on platinum (100) and (111) oriented nanosurfaces. Electrochem Commun 2012;22:109–12.
[51] Chen Y, Shi J, Chen S. Small-molecule (CO, H2) electro-oxidation as an electrochemical tool for characterization of Ni@Pt/C with different Pt coverages. J Phys Chem C 2015;119:7138–45.
[52] Ochal P, Gomez de la Fuente JL, Tsypkin M, Seland F, Sunde S, Muthuswamy N, et al. CO stripping as an electrochemical tool for characterization of Ru@Pt core-shell catalysts. J Electroanal Chem 2011;655:140–6.
[53] Ye Y, Joo J, Lee S, Lee J. A direct one-step synthetic route to Pd-Pt nanostructures with controllable shape, size, and composition for electrocatalytic applications. J Mater Chem A 2014;2:19239–46.
[54] Guillén-Villafuerte O, García G, Orive AG, Anula B, Creus AH, Pastor E. Electrochemical characterization of 2D Pt nanoislands. Electrocatalysis 2011;2:231.
[55] Guerin S, Hayden BE, Lee CE, Mormiche C, Owen JR, Russell AE, et al. Combinatorial electrochemical screening of fuel cell electrocatalysts. J Comb Chem 2004;6:149–58.
[56] García G, Koper MTM. Dual reactivity of step-bound carbon monoxide during oxidation on a stepped platinum electrode in alkaline media. J Am Chem Soc 2009;131:5384–5.
[57] García G, Koper MTM. Carbon monoxide oxidation on Pt single crystal electrodes: understanding the catalysis for low temperature fuel cells. ChemPhysChem 2011;12:2064–72.
[58] García G, González-Orive A, Roca-Ayats M, Guillén-Villafuerte O, Planes GÁ, Martínez-Huerta MV, et al. Platinum border atoms as dominant active site during the carbon

monoxide electrooxidation reaction. Int J Hydrogen Energy 2016;41:19674–83.
[59] García G, Rodríguez P, Rosca V, Koper MTM. Fourier transform infrared spectroscopy study of CO electro-oxidation on Pt(111) in alkaline media. Langmuir 2009;25:13661–6.
[60] Garcia G, Koper MTM. Stripping voltammetry of carbon monoxide oxidation on stepped platinum single-crystal electrodes in alkaline solution. Phys Chem Chem Phys 2008;10:3802–11.
[61] Brimaud S, Pronier S, Coutanceau C, Léger JM. New findings on CO electrooxidation at platinum nanoparticle surfaces. Electrochem Commun 2008;10:1703–7.
[62] Urchaga P, Baranton S, Coutanceau C, Jerkiewicz G. Electro-oxidation of COchem on Pt nanosurfaces: solution of the peak multiplicity puzzle. Langmuir 2012;28:3658–63.
[63] Flórez-Montaño J, García G, Guillén-Villafuerte O, Rodríguez JL, Planes GA, Pastor E. Mechanism of ethanol electrooxidation on mesoporous Pt electrode in acidic medium studied by a novel electrochemical mass spectrometry set-up. Electrochim Acta 2016;209:121–31.
[64] Esterle TF, Russell AE, Bartlett PN. Study of carbon monoxide oxidation on mesoporous platinum. ChemPhysChem 2010;11:2896–905.
[65] Solla-Gullón J, Vidal-Iglesias FJ, Herrero E, Feliu JM, Aldaz A. CO monolayer oxidation on semi-spherical and preferentially oriented (100) and (111) platinum nanoparticles. Electrochem Commun 2006;8:189–94.
[66] Friedrich KA, Henglein F, Stimming U, Unkauf W. Size dependence of the CO monolayer oxidation on nanosized Pt particles supported on gold. Electrochim Acta 2000;45:3283–93.
[67] Maillard F, Eikerling M, Cherstiouk OV, Schreier S, Savinova E, Stimming U. Size effects on reactivity of Pt nanoparticles in CO monolayer oxidation: the role of surface mobility. Faraday Discuss 2004;125:357–77.
[68] Fashedemi OO, Ozoemena KI. Comparative electrocatalytic oxidation of ethanol, ethylene glycol and glycerol in alkaline medium at Pd-decorated FeCo@Fe/C core-shell nanocatalysts. Electrochim Acta 2014;128:279–86.
[69] Liu Z, Hong L. Electrochemical characterization of the electrooxidation of methanol, ethanol and formic acid on Pt/C and PtRu/C electrodes. J Appl Electrochem 2007;37:505–10.
[70] Cai J, Zeng Y, Guo Y. Copper@palladium–copper core–shell nanospheres as a highly effective electrocatalyst for ethanol electro-oxidation in alkaline media. J Power Sources 2014;270:257–61.
[71] Yang G, Zhou Y, Pan H-B, Zhu C, Fu S, Wai CM, et al. Ultrasonic-assisted synthesis of Pd–Pt/carbon nanotubes nanocomposites for enhanced electro-oxidation of ethanol and methanol in alkaline medium. Ultrason Sonochem 2016;28:192–8.
[72] Armstrong RC, Wolfram C, de Jong KP, Gross R, Lewis NS, Boardman B, et al. The frontiers of energy. Nat Energy 2016;1:15020.